catalysts

MDPI

Article

Solar-Driven Selective Benzyl Alcohol Oxidation in Pickering Emulsion Stabilized by CNTs/GCN Hybrids Photocatalyst

Yunyi Han [1], Yuwei Hou [1], Xuezhong Gong [1,*], Yu Zhang [1], Meng Wang [1], Pekhyo Vasiliy Ivanovich [1], Meili Guan [2] and Jianguo Tang [1,*]

[1] Institute of Hybrid Materials, National Center of International Research for Hybrid Materials Technology, National Base of International Science & Technology Cooperation, College of Materials Science and Engineering, Qingdao University, Qingdao 266071, China; hanyunyi6688@163.com (Y.H.); houyuwei3114@163.com (Y.H.); yzhang_000@126.com (Y.Z.); wangmeng0_00@163.com (M.W.); vpekhno@163.com (P.V.I.)

[2] College of Chemical and Biological Engineering, Shandong University of Science and Technology, Qingdao 266590, China; mlguan@sdust.edu.cn

* Correspondence: xzgong@qdu.edu.cn (X.G.); tang@qdu.edu.cn (J.T.)

Abstract

Herein, a bi-functional composite photocatalyst was synthesized by integrating carbon nanotubes (CNTs) and graphitic carbon nitride (GCN) via a facile electrostatic self-assembly strategy. The resulting CNTs/GCN composite served dual roles as both a solid emulsifier and a photocatalyst, enabling highly efficient photocatalytic benzyl alcohol oxidation within a Pickering emulsion system. The relationship between emulsion droplet size and solid emulsifier dosage was investigated and optimized. The enhanced photocatalytic function was supported by an improved photocurrent response and reduced charge-transfer resistance, attributed to superior charge separation efficiency. Consequently, the benzyl alcohol conversion efficiency achieved in the Pickering emulsion system (58.9%) was three-fold of that observed in a traditional oil–water non-emulsion system (19.0%). Key active species were identified as photoholes, and an interfacial reaction mechanism was proposed. This work provides a new approach for extending photocatalytic applications in aqueous environments to diverse organic conversion reactions through the construction of multifunctional photocatalysts.

Keywords: polymeric carbon nitride; carbon nanotubes; benzyl alcohol; Pickering emulsion; photocatalysis

check for updates

Academic Editor: Ermete Antolini

Received: 29 June 2025
Revised: 29 July 2025
Accepted: 3 August 2025
Published: 7 August 2025

Citation: Han, Y.; Hou, Y.; Gong, X.; Zhang, Y.; Wang, M.; Ivanovich, P.V.; Guan, M.; Tang, J. Solar-Driven Selective Benzyl Alcohol Oxidation in Pickering Emulsion Stabilized by CNTs/GCN Hybrids Photocatalyst. *Catalysts* **2025**, *15*, 753. https://doi.org/10.3390/catal15080753

Copyright: © 2025 by the authors. Licensee MDPI, Basel, Switzerland. This article is an open access article distributed under the terms and conditions of the Creative Commons Attribution (CC BY) license (https://creativecommons.org/licenses/by/4.0/).

1. Introduction

Photocatalytic oxidation offers a promising green approach for organic synthesis and resource transformation. Aromatic aldehydes and their derivatives are highly valuable intermediates in medicine and food fields-related fine chemistry [1]. They are industrially produced via a traditional chemical oxidation method, which is efficient but has high costs and is environmentally unfriendly, thus failing to meet the standards of green chemical production [2]. As an advanced oxidation technology, the photocatalytic selective oxidation of aromatic alcohols to aldehydes demonstrates the most potential and is a promising alternative due to its green and sustainable solar energy input.

Efficient photocatalytic organic transformations require sufficient contact between the organic substrate and catalyst. However, most reported photocatalysts are hydrophilic and thus exhibit poor affinities toward organic substrates. In this context, Pickering emulsions

offer an ideal catalytic platform where the photocatalyst acts as a solid emulsifier, dispersing at the oil-in-water or water-in-oil interface. The so-called Pickering emulsion has been popularly applied in food and cosmetics chemistry [3]. Compared with conventional emulsions, Pickering emulsions offer significant advantages: solid emulsifier particles are reusable, environmentally benign, and economically advantageous. However, stabilizing the oil–water interface necessitates photocatalytic particles with interfacial activity (surface amphiphilicity). Consequently, the design and fabrication of amphiphilic photocatalysts have emerged as a critical research focus.

Graphitic carbon nitride (GCN) is a polymeric photocatalyst with a bandgap of 2.7 eV and appropriate CB and VB potential [4]. It has been widely applied in various photocatalytic reactions, e.g., water splitting [5], CO_2 reduction [6], pollutant degradation [7,8] and so on. In the ideal structure of GCN, its hydrophobic conjugated framework (composed of heptazine rings) and hydrophilic terminal groups (–NH or $–NH_2$) confer inherent amphiphilicity. Xu et al., for the first time, reported that GCN prepared via the thermal polymerization of melamine-cyanuric acid supramolecular aggregates can function as an effective Pickering emulsifier [9]. It demonstrates excellent stability in various immiscible oil–water systems, including cyclohexane/water, toluene/water, and heptane/water. Yang et al. developed Pd/GCN as new solid emulsifier to position catalytic sites at the oil–water interface for improving nitroarenes reduction reaction efficiency in a biphasic system [10]. These reported outcomes primarily stem from the inherent amphiphilicity of graphitic carbon nitride. However, during its practical synthesis, the inevitable introduction of defects and oxygen-containing functional groups (e.g., C=O, –OH) shifts its surface properties towards a predominantly hydrophilic nature, thereby diminishing the hydrophobic component essential for balanced amphiphilicity.

Carbon nanotubes (CNTs) have attracted considerable interest due to their unique structural features and exceptional electrical conductivity [11–14]. The incorporation of CNTs not only enhances the light absorption capacity of the composite photocatalyst (as CNTs function as light-harvesting materials) [15] but also facilitates the separation of photogenerated electron–hole pairs (owing to the superior conductivity of CNTs) [16,17]. Moreover, it modulates the hydrophobicity of the hybrid through their large conjugated hydrophobic structures. Consequently, the hybrid coupling of CNTs and GCN endows the composite photocatalyst with enhanced multi-functionality.

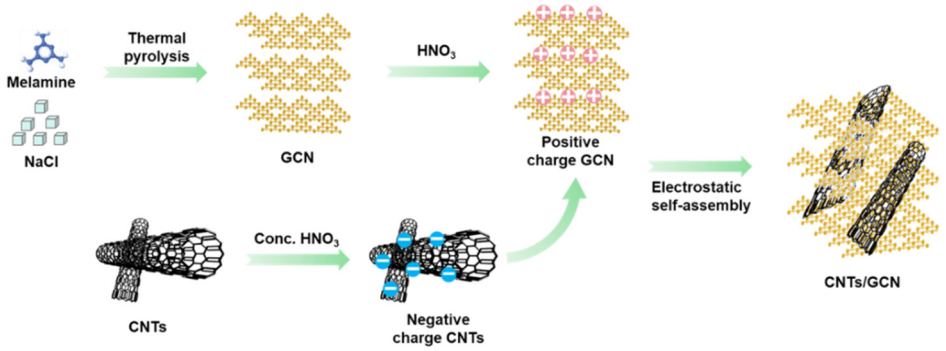
In this study, CNTs/GCN hybrids were obtained via electrostatic self-assembly and applied for the photocatalytic selective oxidation of benzyl alcohol in Pickering emulsions. A biphasic system was constructed using benzyl alcohol as the oil phase and CNTs/GCN composites as stabilizers/catalysts. The relationship between emulsifier dosage and emulsion droplet size was systematically investigated. Remarkably, the CNTs/GCN-1 composite demonstrated an efficient photocatalytic conversion of benzyl alcohol when serving as both emulsifier and photocatalyst for the Pickering emulsion. This enhanced performance originated from the hydrophilic–phobic balance established between hydrophobic CNTs and hydrophilic GCN, which strengthened the affinity of benzyl alcohol on the CNTs/GCN hybrid. This work provides novel insights into the design of CNTs (or other material)-modified binary composites for photocatalytic applications in Pickering emulsion systems.

2. Results and Discussion

2.1. Morphology and Structure

It is reported that the thermal pyrolysis of melamine in the presence of NaCl would introduce Na^+ in the structure even after washing, and the Na^+ could be exchanged by protons or cations [18,19]. So, it is reasonable that the GCN undergoes ion exchange with protons during the HNO_3 treatment and thus, exhibits a positive charge

(ζ = 55 mV). (Figure S1). The CNTs exhibit negative surface charges (ζ = −29 mV) after nitric acid treatment, since surface carboxylic groups are introduced [20]. Hence, the opposite charges allow the GCN and CNTs to assemble into stable composites via electrostatic interaction [21] (Scheme 1). Furthermore, the CNTs/GCN hybrid also showed a high absolute zeta potential value (ζ = 42.7 mV), suggesting a strong electrostatic repulsion between particles, which prevents aggregation in aqueous suspension. Maintaining a stable and well-dispersed suspension is essential for maximizing the accessible surface area of the hybrid photocatalyst and incident light and further contributes directly to its superior photocatalytic activity.



Scheme 1. Schematic diagram of CNTs/GCN hybrid materials prepared by electrostatic assembly.

SEM and TEM images revealed the surface morphology and microstructure of pristine GCN and CNTs/GCN hybrids. As shown in the SEM images (Figure 1a), pristine GCN exhibits an aggregated block-like morphology with dimensions of approximately 5 μm. Notably, Figure 1b clearly demonstrates the penetration of CNTs through the GCN matrix. TEM observations (Figure 1c,d) further reveal that the GCN consists of stacked two-dimensional (2D) nanosheets with lateral sizes of around 1 μm [22]. The CNTs are intimately intertwined with the GCN layers, displaying diameters of 20–80 nm and lengths spanning several micrometers. These structural features provide direct visual evidence for the successful hybridization of CNTs with GCN.

The crystal structure of the hybrids was determined by XRD, as shown in Figure 2a. For pristine GCN, two distinct XRD peaks are observed at 13.4° and 27.4°. The intense peak at 27.4° is assigned to the (002) plane of carbon nitride (d = 0.322 nm), indicative of the graphitic interlayer stacking microstructure. The peak at 13.4° corresponds to the (100) plane (d = 0.655 nm), which is assigned to the in-plane ordering of tri-s-triazine units [23]. In the CNTs/GCN hybrids, the intense peak of the (002) plane shifted to 27.8°. This may be caused by the nitric acid treatment (Figure S2). The CNTs showed a diffraction peak at 25.6°, corresponding to the (002) plane of the graphitic-like structure (Figure S3). However, there no discernible diffraction peaks of the CNTs were observed in the hybrids. This is likely due to the weak intensity and overlap by the dominant GCN matrix [24]. Notably, the preservation of these characteristic peaks of GCN confirms that the electrostatic assembly process does not disrupt the crystalline structure of GCN.

The functional groups of pristine GCN and CNTs/GCN-*x* hybrids were characterized by FT-IR spectroscopy. As shown in Figure 2b, all CNTs/CN-*x* hybrids exhibit FT-IR spectra analogous to pristine GCN. The broad absorption band at 3000–3300 cm^{-1} arises from N–H and O–H stretching vibrations [25], confirming the retention of amino functional groups. The multi-peaks within 1228–1632 cm^{-1} are attributed to the in-plane stretching modes of heterocyclic C–N and C=N bonds in the GCN framework [26,27]. The sharp band at 796 cm^{-1} corresponds to the breathing mode of triazine units [28]. The FT-IR spectra also demonstrated that the hybridization process did not alter the fundamental structure

of GCN. This conclusion aligns with XRD observations, further validating the structural integrity of the hybrids.

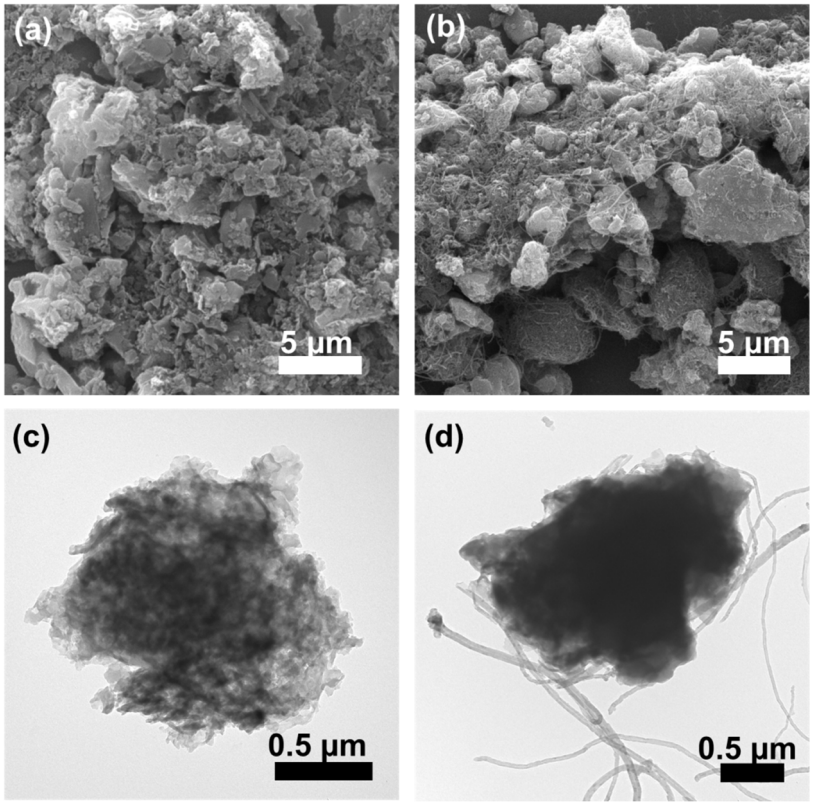


Figure 1. SEM and TEM images of (**a**,**c**) pristine GCN and (**b**,**d**) CNTs/GCN-1.

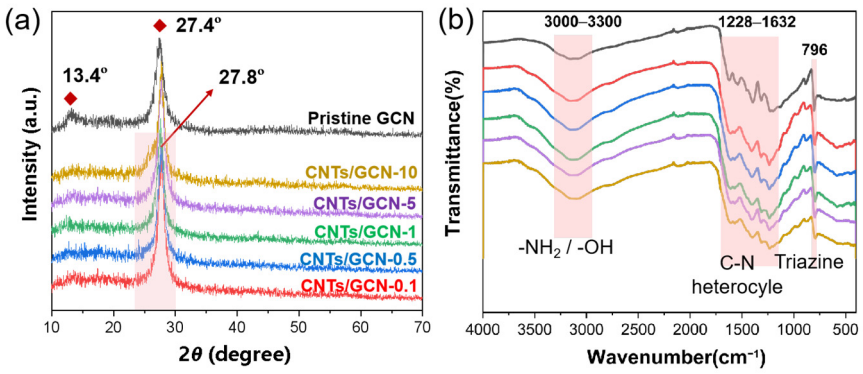


Figure 2. (**a**) XRD pattern and (**b**) FT-IR spectra of pristine GCN and CNTs/GCN hybrids.

X-ray photoelectron spectroscopy (XPS) measurements confirm the elemental composition and chemical states of the CNTs/GCN composites. In the survey spectrum (Figure 3a), for the elements of C, N, O, and Cl can be found. The Cl originates from the NaCl source during the synthesis process. The O arises from the nitric acid treatment, by which the GCN was partially oxidized [29]. The high-resolution C1s XPS spectrum (Figure 3b) reveals three distinct binding energy peaks at 284.8 eV, 285.8 eV, and 287.7 eV, corresponding to the sp^2 C in CNTs, C–O bonds, and the sp^2 C in N–C=N configurations, respectively [30]. The high resolution N1s spectrum can be deconvoluted into three peaks at 398.4 eV, 399.7 eV, and 400.9 eV, respectively (Figure 3c), which correspond to C-N=C, -NH_2, and C-NH_x [31].

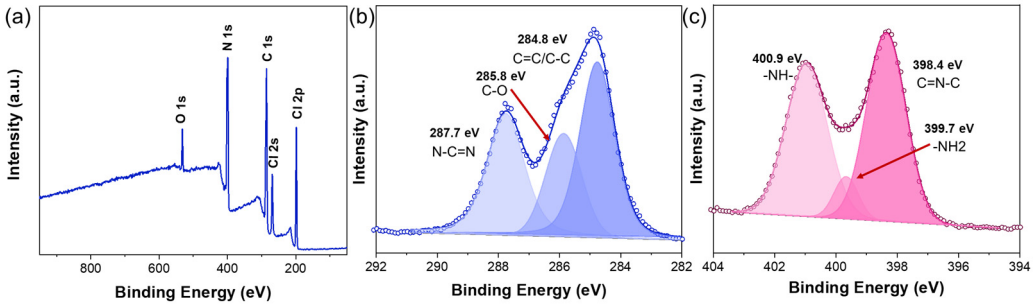


Figure 3. (**a**) XPS spectra for CNTs/GCN-1; (**b**) full survey and high resolution of C 1s. (**c**) full survey and high resolution of N 1s.

2.2. Optical Properties

The UV-Vis diffuse reflectance spectra (DRS) of the hybrid samples are presented in Figure 4a. Pristine GCN exhibits an obvious absorption edge at 450 nm, corresponding to its intrinsic bandgap [4]. Notably, the CNTs/GCN hybrids demonstrate an enhanced light absorption intensity in the 450–800 nm range compared with pristine GCN, suggesting an improved light-harvesting capability that may contribute to enhanced photocatalytic activity. Increasing the CNTs loading progressively strengthens the visible-light absorption intensity of the CNTs/GCN-x composites, attributed to the broadband light absorption properties of CNTs. However, excessive CNTs content (>10 wt%) leads to significant sample darkening (Figure S4), which may hinder light penetration and reduce effective photon utilization [32]. Hence, the optimum CNTs content in the hybrids should be critically optimized by other characterizations and measurements, as will be discussed below.

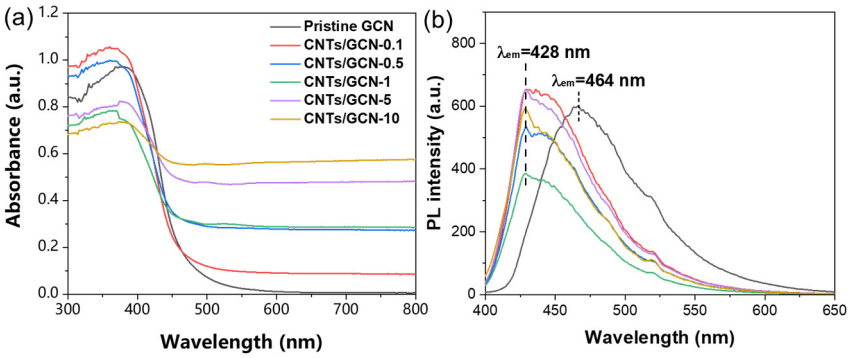


Figure 4. (**a**) UV-Vis absorption spectra and (**b**) PL emission spectra (solid-state) of pristine GCN and CNTs/GCN-X hybrids. Excitation at 380 nm.

The separation efficiency of photogenerated charges critically determine the photocatalytic performance of semiconductor materials [33]. In general, the photoluminescence (PL) intensity of a photocatalyst inversely correlates with its charge separation efficiency, as lower PL signals indicate suppressed recombination of photogenerated electron–hole pairs [34]. As evidenced by the PL spectra in Figure 4b, all CNTs/GCN hybrids exhibit significantly reduced fluorescence intensity compared with pristine GCN. Notably, the CNTs/GCN-1 composite demonstrates the lowest PL intensity, reflecting the highest charge separation efficiency among the series [35]. This phenomenon is attributed to the introduction of CNTs, which serve as electron-conducting pathways to facilitate interfacial charge transfer and inhibit the recombination of photogenerated carriers. It should be noted that the PL emission peak of CNTs/GCN hybrids shifted to 428 nm compared with pristine GCN (464 nm). It should be ascribed to the quantum size effect that is caused by the reduced dimension after the nitric acid treatment of GCN [29]. In all, the optical properties

of the CNTs/GCN reflected an enhanced light-harvest capability and charge separation efficiency and is expected to show optimized photocatalytic activity.

2.3. Photoelectrochemical Performance

To investigate the photophysical behavior of photogenerated charge carriers in CNTs/GCN hybrids, PEC measurement was conducted. The transient photocurrent response is shown in Figure 5a. The CNTs/GCN-x samples all exhibit improved photocurrent, while the CNTs/GCN-1 showed the highest photocurrent density (8.7 μA cm^{-2}), with a 5-fold enhancement compared with pristine GCN (1.7 μA cm^{-2}). The CNT sample only exhibits a negligible photocurrent density (1.02 μA cm^{-2}) (Figure S5). The EIS Nyquist plots (Figure 5b) reveal that the semicircular radius of all the CNTs/GCN-x hybrids is smaller than that of pristine GCN, suggesting lower charge transfer resistance, which likely contributes to faster charge transfer kinetics. The resistance is lower with increased CNT content among the CNTs/GCN hybrids, which is likely due to the perfect conductivity of CNTs. These results further confirm the effective separation of photoinduced electrons and holes and is consistent with the previous PL results.

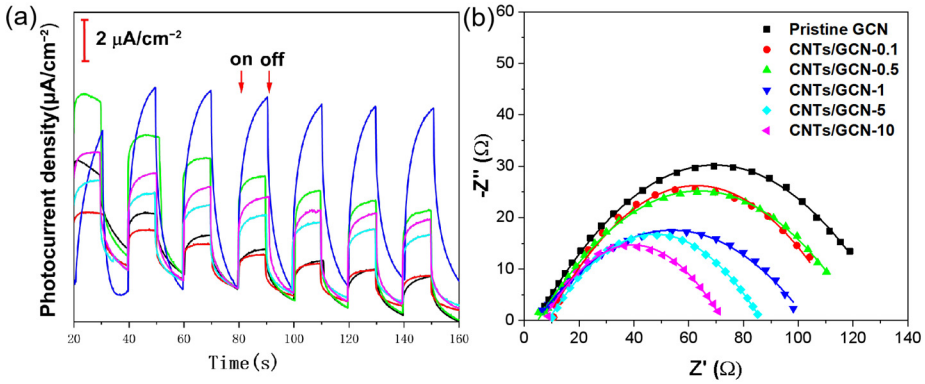


Figure 5. (**a**) Transit photocurrent response and (**b**) EIS of pristine GCN and CNTs/GCN-x samples.

2.4. CNTs/GCN Stabilized Pickering Emulsion

The Pickering emulsion is stabilized by solid particles that spread at the oil/water interface. The assembling of the particles at the interface can be single/multiple layers or even net-like linking, depending on the emulsifier amount and morphology [36] (Figure 6a). In this study, the CNTs/GCN hybrid-stabilized oil-in-water type Pickering emulsion was obtained and is illustrated in Figure 6b. The droplet size is a critical factor influencing emulsion stability. Smaller droplet size corresponds to a larger oil–water contact interface and enhanced mass/heat transfer processes, which are crucial for catalytic reactions [37]. Herein, the CNTs/GCN-1 was selected as an emulsifier to perform the Pickering emulsion, and the relationship between droplet size and photocatalyst amount was investigated.

As shown in Figure 6c–h, the droplet morphology differs significantly depending on the amount of emulsifier used. With increasing solid particle content from 0.2 mg mL^{-1} to 1 mg mL^{-1}, the droplet size decreases sharply from 55.34 μm ± 2.5 to 27.75 μm ± 3.2. Further increasing the emulsifier amount to 10 mg mL^{-1}, the droplet size exhibits a slight increase [38,39]. It is in accordance with the previous report that as the solid particle concentration increases, the mechanical resistance and repulsive force between the particles at the droplet interface counteracts shear forces, resulting in the maintenance of larger droplet sizes.

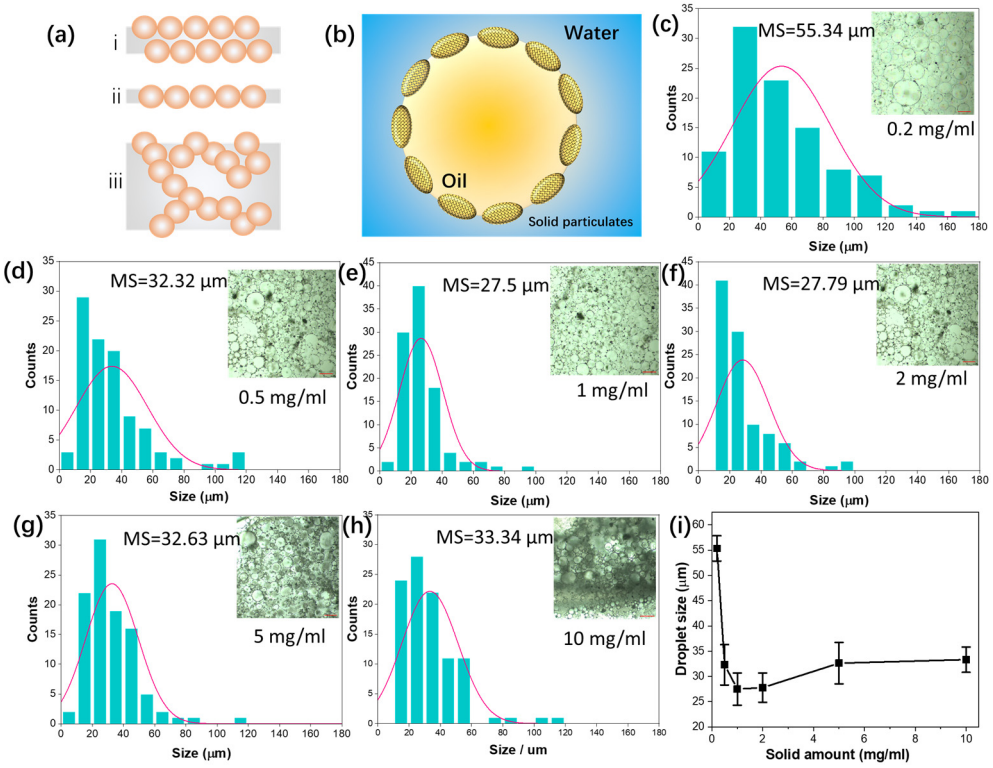


Figure 6. (**a**) Models of Pickering emulsifier distribution (**i**–**iii**). (**b**) Illustration of o/w type emulsion stabilized by the CNTs/GCN-1 hybrid. (**c**–**h**) Size fraction of emulsion droplets formed by different amounts of emulsifier, the inset is a microscope photograph of the emulsion with a scale bar of 100 μm; (**i**) the relationship between the emulsion droplet size and the emulsifier dosage. Error bars represent the standard deviation (SD) of 100 droplets from the optical images.

2.5. Photocatalytic Benzyl Alcohol Oxidation in Pickering Emulsion

To validate the effectiveness of the emulsion-based photocatalytic reaction, three kinds of reaction systems were adapted: CNTs/GCN-1 stabilized emulsion, GCN stabilized emulsion, and non-emulsified biphase. Benzyl alcohol was selected as the organic substrate to evaluate the photocatalytic activity of the hybrids. After 4 h of irradiation, only benzyl aldehyde was detected as the predominant product, indicating 100% selectivity of BA oxidation (Figure S6). The conversion efficiency (CE) reached 19.02% in the non-emulsified biphasic system (Figure 7a). In contrast, the CE reached 58.9% in the CNTs/GCN-1 stabilized emulsion. Although the pristine GCN is capable of forming emulsion, the CE can only reach 31.64%, which is much lower than that of CNTs/GCN-stabilized emulsion. This marked improvement confirms that emulsification-induced interfacial engineering between BA and the photocatalyst in water critically enhances reaction efficiency [40]. Moreover, the CNTs/GCN hybrid exhibits superior photocatalytic activity for the Pickering emulsion-catalyzed oxidation of benzyl alcohol compared with pristine GCN. This enhancement originates from the role of CNTs with two aspects: increased hydrophobicity and enhanced charge separation efficiency of the hybrid. The former contributes to the higher affinity of BA to the hybrid surface than less hydrophobic pristine GCN (Figure S7). The latter benefits from the hybridized CNTs that accelerate the photogenerated electrons' transport kinetics and thus leave more net holes for oxidation reaction.

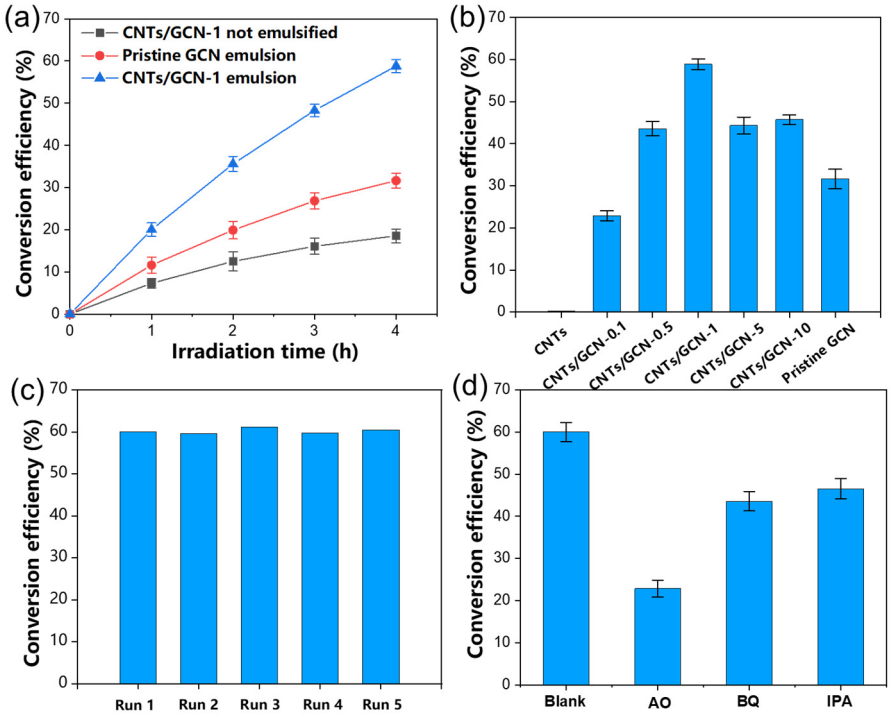


Figure 7. (**a**) Conversion efficiency of benzyl alcohol in the three different systems; (**b**) the conversion efficiency of different samples after 4 h irradiation; (**c**) the conversion efficiency of the 5 cycle tests; (**d**) Free radical capture experiments.

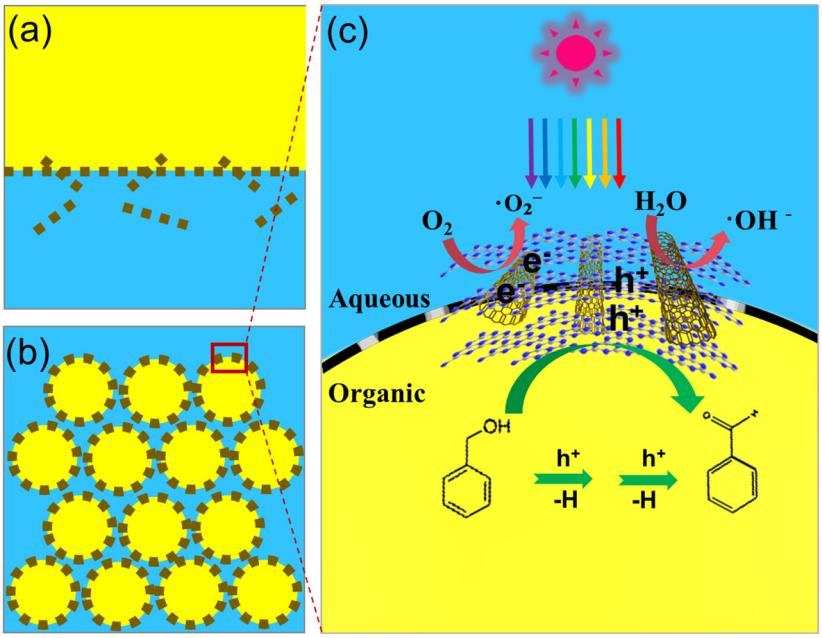
Based on the optimized emulsion system, photocatalytic BA conversion efficiency over different hybrids was performed, as shown in Figure 7b. All the hybrids showed improved CE towards BA oxidation under 4 h irradiation, compared with pristine GCN (Table S1). The CNTs/GCN-1 showed the highest CE (59.2%), which is consistent with the PEC measurement. The photocatalyst can be easily recovered and cyclically used after the reaction by centrifuging the emulsion and re-dispersing it in the oil/water system. Thus, the recyclability of the hybrids was performed, and the CE in each cycle was listed, as shown in Figure 7c, the CE of BA did not decrease significantly after 5 cycles, highlighting the excellent reusability of the emulsion photocatalytic system [41]. In addition, the characterizations of the CNTs/GCN-1 after the photocatalysis reaction showed that there was no crystalline structure deformation or functional group loss (Figure S8), confirming stability against repeated utilization.

2.6. Proposed Photocatalytic Mechanism

To gain deeper insights into the roles of photoactive species in the photocatalytic oxidation of benzyl alcohol, a series of radical trapping experiments were conducted, with results presented in Figure 7d. Ammonium oxalate (AO), 1,4-benzoquinone (BQ), and isopropanol (IPA) were employed as sacrificial agents for photogenerated holes (h^+), superoxide radicals ($\cdot O_2^-$), and hydroxyl radicals ($\cdot OH^-$), respectively [42]. In the presence of these scavengers, the benzyl alcohol conversion efficiency decreased significantly to 23% (AO), 43% (BQ), and 45% (IPA), demonstrating the critical involvement of $\cdot O_2^-$, h^+, and $\cdot OH^-$ in the reaction process. Among these, h^+ played the predominant role [43]. Notably, benzaldehyde selectivity remained at nearly 100% across all photocatalytic oxidation reactions [44]. This exceptional selectivity arises from the thermodynamically controlled oxidation pathway of benzyl alcohol to benzaldehyde, which is intrinsically linked to the energy band structure of the photocatalyst. The valence band position of GCN is approximately 1.6 eV; the driving force to oxidize benzyl alcohol to benzaldehyde (+0.9 eV)

is much higher than that of benzaldehyde to benzoic acid (>1.3 eV). Although the potential of the photohole is theoretically sufficient, the kinetics of this second oxidation step appear to be unfavorable in this system. In all, the large difference in required oxidation potentials (~0.6–0.8 V) between the benzyl alcohol→benzaldehyde and benzaldehyde→benzoic acid steps provides a fundamental thermodynamic/kinetic window where the first oxidation is rapid, while the second is suppressed, leading to the observed high selectivity for benzaldehyde accumulation.

Therefore, the mechanism of emulsion-photocatalytic benzyl alcohol oxidation is proposed as below: compared with the non-emulsified biphasic system in which the photocatalyst randomly spread along the solo oil/water interface (Scheme 2a), the CNTs/GCN hybrids dispersed outside of each oil droplet in the emulsion system (Scheme 2b). Obviously, the increased interface area becomes a prerequisite for the improvement of the photocatalytic reaction efficiency. Upon light irradiation, the GCN in the CNTs/GCN hybrid is excited to generate electron–hole pairs. The photogenerated electrons migrate to CNTs via the CNTs-GCN interface. Owing to the exceptional conductivity of CNTs, these electrons are rapidly transported away, effectively suppressing charge recombination. Subsequently, the electrons are scavenged by dissolved oxygen to generate superoxide radicals ($\cdot O_2^-$), the primary active species responsible for oxidizing benzyl alcohol adsorbed on the photocatalyst surface. Concurrently, the photogenerated holes (h^+) react with the adsorbed benzyl alcohol to form benzaldehyde through the deprotonation process [45].



Scheme 2. Illustration of (**a**) non-emulsion and (**b**) emulsion photocatalytic system for photocatalyst dispersed in the medium. (**c**) The proposed photocatalytic mechanism for benzyl alcohol oxidation in Pickering emulsion.

3. Experimental Section

3.1. Chemicals

All the raw materials were procured from commercial suppliers and, unless otherwise specified, were utilized without further purification. Specifically, multi-wall carbon nanotube (AR) and dicyandiamide (AR) were obtained from Shanghai MacLean Chemical Co., Ltd. (Shanghai, China). Additionally, Nitric acid (AR) and Benzyl alcohol (AR) were sourced from Sinopharm Group Chemical Reagent Co., Ltd. (Shanghai, China).

3.2. Preparation of CNTs/GCN Hybrid Material

3.2.1. Synthesis of GCN

Polymerized GCN sheets were synthesized using dicyandiamide as the precursor [46]. Specifically, 2 g of dicyandiamide and 20 g NaCl was ground and mixed in a mortar. placed in a crucible and heated in a muffle furnace at a heating rate of 2.2 °C/min to 550 °C, followed by a 4 h holding period at this temperature. After cooling down to room temperature, the product was washed by copies of DI water to remove the excess NaCl salt. Finally, the solid was dried in an oven, and the yellow powder denoted as GCN.

3.2.2. Synthesis of CNTs/GCN Hybrid

The CNTs were firstly treated with nitric acid to introduce a negatively charged surface. Typically, 10 mg of CNTs was dispersed in nitric acid (5 mL, 69 wt%) via ultrasonication for 1 h, followed by being magnetically stirred for 6 h to be oxidized. Meanwhile, the GCN powder was dispersed in another 5 mL of nitric acid (69 wt%) and ultrasonicated for 1 h to form a homogeneous suspension. Afterwards, the treated GCN and CNTs suspension were mixed according to the desired ratio, followed by being centrifuged and washed with DI water. The final precipitate was dried in an oven and labeled as CNTs/GCN-x, where x = 0.1, 0.5, 1, 5, and 10, representing the CNTs' content (wt%) in the hybrids.

3.3. Characterization

The crystal structures of the synthesized samples were analyzed by X-ray diffraction (XRD) using Cu Kα radiation (Bruke, Germany) with a scanning rate of $4^{\circ}\cdot min^{-1}$. The morphological features of the products were investigated using scanning electron microscopy (SEM) and transmission electron microscopy (TEM). UV-Vis diffuse reflectance spectra (DRS) were recorded on a UV-750s spectrophotometer (Thermo Fisher, Beijing, China) Fourier-transform infrared (FT-IR) spectra were acquired on an FT-IR spectrometer (Thermo Fisher, Beijing, China) Photoluminescence (PL) spectra were measured using a fluorescence spectrophotometer with an excitation wavelength of 380 nm. X-ray photoelectron spectroscopy (XPS) analysis was performed on a VG ESCALAB MK system (Thermo Fisher, Beijing, China) equipped with an Al Kα X-ray source (hv = 1486.6 eV).

3.4. Photoelectrochemical Measurement

Photoelectrochemical measurements (photocurrent response and electrochemical impedance spectroscopy (EIS)) were performed using an electrochemical workstation. To prepare the working electrode, the catalyst sample (4 mg) was homogenized with ethanol (2 mL) and Nafion solution (10 µL) via ultrasonication to form a uniform suspension. The catalyst suspension was then drop-casted onto a pre-cleaned FTO glass substrate (1 × 4 cm). A three-electrode system was employed, with a platinum wire as the counter electrode, a Ag/AgCl electrode as the reference electrode, and samples on FTO as the working electrode; 0.2 $mol\cdot L^{-1}$ Na_2SO_4 aqueous solution was used as the electrolyte. For photocurrent measurements, a 300 W Xeon lamp (Microenerg, Beijing, China) was used as the light source, positioned 5 cm from the working electrode surface. EIS was conducted under the same three-electrode configuration with an AC amplitude of 5 mV over a frequency range of 10^{-1} to 10^{5} Hz.

3.5. Preparation of Pickering Emulsion

The Pickering emulsion was prepared through the following procedure: (1) CNTs/GCN-x samples (0.2–10 wt%) were dispersed in 5 mL of water via ultrasonication for 15 min to form the suspension (aqueous phase); (2) n-Hexane (oil phase) was added, followed by homogenization using a vortex mixer at 2000 rpm for 2 min. The morphology of the

emulsion droplet was observed by an optical microscope. The droplet size distributions were quantified using an image analysis software called Nano Measurer 1.2. via processing of microscopic images.

3.6. Photocatalytic Benzyl Alcohol

The photocatalytic experiments were conducted in a quartz glass reactor. Specifically, 15 mg of the prepared photocatalyst was dispersed in 15 mL of deionized water. After ultrasonication to form a homogeneous suspension, 5 mL hexane solvent (oil phase) containing 100 ppm of benzyl alcohol was introduced. A 300 W xenon lamp was employed as the light source. Prior to illumination, the suspension was magnetically stirred in the dark for 30 min to establish an adsorption–desorption equilibrium. Under continuous magnetic stirring, the reaction system was irradiated for 4 h. At 30 min intervals, 2 mL aliquots of the emulsion were withdrawn and centrifuged to separate the solid particles. The upper clear oil solution was collected and analyzed by GC-MS.

4. Conclusions

In this study, CNTs/GCN hybrids were fabricated via a facile electrostatic assembly strategy, and were employed as both an emulsifier and photocatalysts, achieving efficient photocatalytic oxidation of benzyl alcohol in Pickering emulsions. The emulsion droplet size decreased with the increase in photocatalyst, enabling an increased oil/water interface area. The photocatalytic conversion efficiency of benzyl alcohol in the emulsion system was three-fold that of the conventional oil/water biphasic system. This improvement is attributed to the hydrophobic CNTs that promoted the benzyl alcohol affinity to the CNTs/GCN hybrids. Additionally, the CNTs promoted charge separation efficiency by transferring photoelectrons efficiently. This work demonstrates the significant application potential of Pickering emulsions in photocatalytic organic oxidations and presents promising avenues for advancing sustainable oxidation technologies.

Supplementary Materials: The following supporting information can be downloaded at: https://www.mdpi.com/article/10.3390/catal15080753/s1, Figure S1. Zeta potential of GCN, CNTs and CNTs/GCN hybrid after acid treatment; Figure S2. XRD pattern of HNO_3 treated GCN; Figure S3. XRD pattern of CNTs; Figure S4. The optical photo of the GCN and CNTs/GCN-x hybrid samples showing the color changing with different CNTs content. Figure S5. Transit photocurrent response of CNTs; Figure S6. GC-MS spectra of benzyl alcohol and benzaldehyde; Figure S7. Adsorption of benzyl alcohol on the different samples; Figure S8. SEM image, XRD and FT-IR of CNTs/GCN-1 after photocatalytic reaction; Table S1. Conversion efficiency of Benzyl alcohol under different reaction conditions.

Author Contributions: Writing—original draft, Methodology, Data curation, Y.H. (Yunyi Han); Investigation, Y.H. (Yuwei Hou); Visualization, Y.Z.; Validation, M.W.; Validation, P.V.I.; Funding acquisition, M.G.; Supervision, Writing—review and editing, Funding acquisition, X.G.; Project administration, J.T. All authors have read and agreed to the published version of the manuscript.

Funding: This work was financially supported by (1) the National Natural Science Foundation of China for Youths (Grant Nos. 21701057, 21905147), (2) the Natural Science Foundation of Shandong (Grant No. ZR2022MB106) (3) the State Key Project of International Cooperation Research (2023YFE0201100), (4) the Shandong Provincial Key Projects of Double Hundred Foreign Talent Introduction (WSR2023057 and WSR2024062), (5) the National Program for Introducing Talents of Discipline to Universities ("111" plan), and (6) the high level discipline program of Shandong Province of China.

Data Availability Statement: The data are available by request.

Conflicts of Interest: The authors declare no conflicts of interest.

References

1. Linsebigler, L.A.; Lu, G.; Yates, T.J. Photocatalysis on TiO_2 Surfaces: Principles, Mechanisms, and Selected Results. *Chem. Rev.* **2002**, *95*, 735–758. [CrossRef]
2. Giovanni, A.; Vincenzo, A.; Mario, P.; Leonardo, P. Photocatalysis: A promising route for 21st century organic chemistry. *Chem. Comm.* **2007**, *33*, 3425–3437.
3. Wen, J.; Lin, R.; Wu, Y.; Hu, H.; Liu, Z.; Zhou, H.; Ouyang, X. Qualified interlayer modifier for organic solar cells with optimized interfacial topography and boosted efficiency based on biomass-derived acid. *Chem. Eng. J.* **2022**, *450*, 138169. [CrossRef]
4. Wang, X.; Maeda, K.; Thomas, A.; Takanabe, K.; Xin, G.; Carlsson, J.M.; Domen, K.; Antonietti, M. A metal-free polymeric photocatalyst for hydrogen production from water under visible light. *Nat. Mater.* **2009**, *8*, 76–80. [CrossRef]
5. Zhu, X.; Guan, M.; Gong, R.; Gong, X.; Dai, C.; Tang, J. A Conjugated polymer coupled with graphitic carbon nitride for boosting photocatalytic hydrogen generation under visible light. *Sustain. Energy Fuels* **2023**, *7*, 1537–1543. [CrossRef]
6. Gong, X.; Yu, S.; Guan, M.; Zhu, X.; Xue, C. Pyrene-functionalized polymeric carbon nitride for photocatalytic carbonate reduction with simultaneous biphasic oxidation of alkenes. *Mater. Chem. A* **2019**, *7*, 7373–7379. [CrossRef]
7. Gong, R.; Yang, X.; Liu, G.; Dong, Z.; Guan, M.; Gong, X.; Tang, J. Tailored polymeric carbon nitride coupled with Bi_2O_3 for constructing Z-Scheme heterojunction with enhanced photocatalytic activity. *ChemPhotoChem.* **2024**, *8*, e202300255. [CrossRef]
8. Yang, X.; Gong, R.; Dong, Z.; Liu, G.; Han, Y.; Hou, Y.; Li, Y.; Guan, M.; Gong, X.; Tang, J. Polymeric Carbon Nitride-CNTs-Ferric Oxide All-Solid Z-Scheme Heterojunction with Improved Photocatalytic Activity towards Organic Dye Removal. *Catalysts* **2024**, *14*, 516. [CrossRef]
9. Jingsan, X.; Markus, A. The Performance of Nanoparticulate Graphitic Carbon Nitride as an Amphiphile. *J. Am. Chem. Soc.* **2017**, *139*, 6026–6029. [CrossRef]
10. Hao, Y.; Hao, S.; Li, Q.; Liu, X.; Zou, H.; Yang, H. Metal-Nanoparticles-Loaded Ultrathin g-C_3N_4 Nanosheets at Liquid-Liquid Interfaces for Enhanced Biphasic Catalysis. *ACS Appl. Mater. Interfaces* **2021**, *13*, 47236–47243. [CrossRef]
11. Hong, C.Y.; Shin, H.D.; Uhm, S.H. Super-hydrophobicity of multi-walled carbon nanotubes treated by a glow discharge. *Surf. Coat. Technol.* **2007**, *201*, 5025–5029. [CrossRef]
12. Xu, Z.; Li, H.; Fu, M. Nitrogen-doped carbon nanotubes synthesized by pyrolysis of nitrogen-rich metal phthalocyanine derivatives for oxygen reduction. *J. Mater. Chem.* **2012**, *22*, 18230–18236. [CrossRef]
13. Rivadulla, F.; Mateo-Mateo, C.; Correa-Duarte, M.A. Layer-by-Layer Polymer Coating of Carbon Nanotubes: Tuning of Electrical Conductivity in Random Networks. *J. Am. Chem. Soc.* **2010**, *132*, 3751–3755. [CrossRef]
14. Dai, H. Carbon nanotubes: Opportunities and challenges. *Sur. Sci.* **2002**, *500*, 218–241. [CrossRef]
15. Nikolaos, K.; Nikos, T.; Dimitrios, T. Current Progress on the Chemical Modification of Carbon Nanotubes. *Chem. Rev.* **2010**, *110*, 5366–5397. [CrossRef]
16. Yu, J.; Ma, T.; Liu, S. Enhanced photocatalytic activity of mesoporous TiO_2 aggregates by embedding carbon nanotubes as electron-transfer channel. *Phys. Chem. Chem. Phys.* **2011**, *13*, 3491–3501. [CrossRef] [PubMed]
17. Feng, C.; Jiang, L.Y. Investigation of uniaxial stretching effects on the electrical conductivity of CNT-polymer nanocomposites. *Phys. D Appl. Phys.* **2014**, *47*, 405103. [CrossRef]
18. Zhang, G.; Xu, Y.; Zhu, J.; Li, Y.; He, C.; Ren, X.; Zhang, P.; Mi, H. Enhanced photocatalytic H_2 production independent of exciton dissociation in crystalline carbon nitride. *Appl. Catal. B-Environ. Energy* **2023**, *338*, 123049. [CrossRef]
19. Yuan, B.; Chu, Z.; Li, G. Water-Soluble Ribbon-Like Graphitic Carbon Nitride (g-C_3N_4): Green Synthesis, Self-Assembly and Unique Optical Properties. *Mater. Chem.* **2014**, *2*, 8212–8215. [CrossRef]
20. Georg, D.S.; Siegmar, R.; Patrick, D.; Andrew, M.; Ralf, G.; Lothar, L.; Norbert, N. Modification of Single-Walled Carbon Nanotubes by Hydrothermal Treatment. *Chem. Mater.* **2003**, *15*, 3314–3319. [CrossRef]
21. Ma, T.; Dai, S.; Jaroniec, M.; Qiao, S. Graphitic Carbon Nitride Nanosheet–Carbon Nanotube Three- Dimensional Porous Composites as High-Performance Oxygen Evolution Electrocatalysts. *Angew. Chem. Int. Ed.* **2014**, *53*, 7281–7285. [CrossRef]
22. Thomas, A.; Fischer, A.; Goettmann, F. Graphitic carbon nitride materials: Variation of structure and morphology and their use as metal-free catalysts. *J. Mater. Chem.* **2008**, *18*, 4893–4908. [CrossRef]
23. Kessler, K.F.; Zheng, Y.; Schwarz, D. Functional carbon nitride materials-design strategies for electrochemical devices. *Nat. Rev. Mater.* **2017**, *2*, 17030. [CrossRef]
24. Guirguis, A.; Polaki, S.R.; Sahoo, G.; Ghosh, S.; Kamruddin, M.; Merenda, A.; Chen, X.; Maina, J.W.; Szekely, G.; Dumee, L. Engineering high-defect densities across vertically-aligned graphene nanosheets to induce photocatalytic reactivity. *Carbon* **2020**, *168*, 32–41. [CrossRef]
25. Nobuaki, T.; Hiromasa, N.; Satoshi, K.; Morinobu, E.; Tsuneo, F. Photochemical deposition of Ag nanoparticles on multi walled carbon nanotubes. *Carbon* **2009**, *47*, 2752–2754.
26. Usman, M.; Zeb, Z.; Ullah, H.; Suliman, M.H.; Humayun, M.; Ullah, L.; Shah, S.N.A.; Ahmed, U.; Saeed, M. A review of metal-organic frameworks/graphitic carbon nitride composites for solar-driven green H_2 production, CO_2 reduction, and water purification. *J. Environ. Chem. Eng.* **2022**, *10*, 107548. [CrossRef]

27. Zhou, L.; Zhang, H.; Sun, H.; Liu, S.; Tade, M.O.; Wang, S.; Jin, W. Recent advances in non-metal modification of graphitic carbon nitride for photocatalysis: A historic review. *Catal. Sci. Technol.* **2016**, *6*, 7002–7023. [CrossRef]
28. Liu, C.; Zhang, Y.; Dong, F.; Reshak, A.H.; Ye, L.; Pinna, N.; Zeng, C.; Zhang, T.; Huang, H. Chlorine intercalation in graphitic carbon nitride for efficient photocatalysis. *Appl. Catal. B Environ.* **2017**, *203*, 465–474. [CrossRef]
29. Wei, H.; Zhang, Q.; Zhang, Y.; Yang, Z.; Zhu, A.; Dionysiou, D.D. Enhancement of the Cr(VI) adsorption and photocatalytic reduction activity of g-C_3N_4 by hydrothermal treatment in HNO_3 aqueous solution. *Appl. Catal. A Gen.* **2016**, *521*, 9–18. [CrossRef]
30. Dresselhaus, M.S.; Jorio, A.; Dresselhaus, G.; Saito, R.; Souza, F.A.G.; Pimenta, M.A. Raman Spectroscopy of Nanoscale Carbons And of An Isolated Carbon Nanotube. *J. Mol. Cryst. Liq. Cryst.* **2002**, *387*, 21–29. [CrossRef]
31. Biesinger, M.C.; Payne, B.P.; Grosvenor, A.P.; Lau, L.W.; Gerson, A.R.; Smart, R.S.C. Resolving surface chemical states in XPS analysis of first row transition metals, oxides and hydroxides: Sc, Ti, V, Cu and Zn. *Appl. Surf. Sci.* **2010**, *257*, 887–898. [CrossRef]
32. Yousefzadeh, S.; Fathi, B. Construction of carbon nanotube-g-C_3N_4 nanocomposite photoanode for the enhanced photoelectrochemical activity in water splitting. *J. Electroanal. Chem.* **2020**, *878*, 114580. [CrossRef]
33. Liu, T.; Pasumarthi, V.; Laporte, C.; Feng, Z.; Li, Q.; Yang, J.; Li, C.; Dupuis, M. Bimodal hole transport in bulk BiVO4 from computation. *J. Mater. Chem. A* **2018**, *6*, 3714–3723. [CrossRef]
34. Yang, T.; Dai, S.; Tan, H.; Zong, Y.; Liu, Y.; Chen, J.; Zhang, K.; Wu, P.; Zhang, S.; Xu, J.; et al. Mechanism of Photoluminescence in Ag Nanoclusters: Metal-Centered Emission versus Synergistic Effect in Ligand-Centered Emission. *J. Phys. Chem. C* **2019**, *123*, 18638–18645. [CrossRef]
35. Dong, Y.; Hu, Q.; Li, B.; Li, X.; Chen, M.; Zhang, M.; Feng, Y.; Ding, Y. Aminated silicon dioxide enriching iron-containing polyoxometalate catalyst confined in CdS for efficient H_2 evolution. *Appl. Catal. B Environ.* **2022**, *304*, 120998. [CrossRef]
36. Eric, D. Food emulsions and foams: Stabilization by particles. *Curr. Opin. Colloid. Interface* **2009**, *15*, 40–49.
37. Tian, Y.; Chang, B.; Lu, J.; Fu, J.; Xi, F.; Dong, X. Hydrothermal synthesis of graphitic carbon nitride-Bi2WO6 heterojunctions with enhanced visible light photocatalytic activities. *ACS App. Mater. Interfaces* **2013**, *5*, 7079–7085. [CrossRef]
38. Binks, B.P.; Clint, J.H. Solid wettability from surface energy components: Relevance to pickering emulsions. *Langmuir* **2002**, *18*, 1270–1273. [CrossRef]
39. Binks, B.P.; Rodrigues, J.A. Inversion of emulsions stabilized solely by ionizable nanoparticles. *Angew. Chem. Int. Ed.* **2005**, *44*, 441–444. [CrossRef]
40. Zhang, L.; Wang, C.; Liu, Y.; Ren, M.; Du, J.; Chen, A.; Li, F. Suppressing interlayer-gliding and Jahn-Teller effect in P_2-type layered manganese oxide cathode via Mo doping for sodium-ion batteries. *Chem. Eng. J.* **2021**, *426*, 130813. [CrossRef]
41. Zhang, Q.; Kong, B.; Liu, H.; Du, X.; Sun, F.; Xia, X. Nanoscale Pickering emulsion food preservative films/coatings: Compositions, preparations, influencing factors, and applications. *Compr. Rev. Food Sci. Food Saf.* **2024**, *23*, e13279. [CrossRef]
42. Shi, Q.; Zhang, X.; Liu, X.; Xu, L.; Liu, B.; Zhang, J.; Xu, H.; Han, Z.; Li, G. In-situ exfoliation and assembly of 2D/2D g-C_3N_4/TiO_2(B) hierarchical microflower: Enhanced photo-oxidation of benzyl alcohol under visible light. *Carbon* **2022**, *196*, 401–409. [CrossRef]
43. Kisch, H.; Bahnemann, D. Best Practice in Photocatalysis: Comparing Rates or Apparent Quantum Yields. *J. Phys. Chem. Lett.* **2015**, *6*, 1907–1910. [CrossRef] [PubMed]
44. Xiao, X.; Zheng, C.; Lu, M.; Zhang, L.; Liu, F.; Zuo, X.; Nan, J. Deficient $Bi_{24}O_{31}Br_{10}$ as a highly efficient photocatalyst for selective oxidation of benzyl alcohol into benzaldehyde under blue LED irradiation. *Appl. Catal. B Environ.* **2018**, *228*, 142–157. [CrossRef]
45. Lima, M.J.; Tavares, P.B.; Silva, A.M.T.; Silva, C.G.; Faria, J.L. Selective photocatalytic oxidation of benzyl alcohol to benzaldehyde by using metal-loaded g-C3N4 photocatalysts. *Catal. Today* **2017**, *287*, 70–77. [CrossRef]
46. Cao, S.; Yu, J. g-C_3N_4-Based Photocatalysts for Hydrogen Generation. *J. Phys. Chem. Lett.* **2014**, *5*, 2101–2107. [CrossRef]

Disclaimer/Publisher's Note: The statements, opinions and data contained in all publications are solely those of the individual author(s) and contributor(s) and not of MDPI and/or the editor(s). MDPI and/or the editor(s) disclaim responsibility for any injury to people or property resulting from any ideas, methods, instructions or products referred to in the content.